tvst

Glaucoma

Comparing Acute IOP-Induced Lamina Cribrosa Deformations Premortem and Postmortem

Junchao Wei[1,*], Yi Hua[1,*], Bin Yang[1,2], Bo Wang[1,3,4], Samantha E. Schmitt[1,5,6], Bingrui Wang[1], Katie A. Lucy[7], Hiroshi Ishikawa[7–9], Joel S. Schuman[7,10,11], Matthew A. Smith[1,3,5,6], Gadi Wollstein[7], and Ian A. Sigal[1,3]

[1] Department of Ophthalmology, University of Pittsburgh, Pittsburgh, PA, USA
[2] Department of Engineering, Duquesne University, Pittsburgh, PA, USA
[3] Department of Bioengineering, University of Pittsburgh, Pittsburgh, PA, USA
[4] Wilmer Eye Institute, Johns Hopkins University School of Medicine, Baltimore, MD, USA
[5] Department of Biomedical Engineering, Carnegie Mellon University, Pittsburgh, PA, USA
[6] Neuroscience Institute, Carnegie Mellon University, Pittsburgh, PA, USA
[7] Department of Ophthalmology, NYU Langone Health, NYU Grossman School of Medicine, New York, NY, USA
[8] Department of Ophthalmology, Casey Eye Institute, Oregon Health & Science University, Portland, OR, USA
[9] Department of Medical Informatics and Clinical Epidemiology, Oregon Health & Science University, Portland, OR, USA
[10] Department of Biomedical Engineering and Electrical and Computer Engineering, New York University Tandon School of Engineering, Brooklyn, NY, USA
[11] Neuroscience Institute, NYU Langone Health, New York, NY, USA

Correspondence: Ian A. Sigal, Laboratory of Ocular Biomechanics, Department of Ophthalmology, University of Pittsburgh School of Medicine, 203 Lothrop Street, Eye and Ear Institute, Rm. 930, Pittsburgh, PA 15213, USA. e-mail: ian@ocularbiomechanics.com

Received: January 15, 2022
Accepted: October 24, 2022
Published: December 1, 2022

Keywords: lamina cribrosa; optic nerve head; digital volume correlation; image registration; glaucoma; biomechanics; strain; exsanguination; intraocular pressure

Citation: Wei J, Hua Y, Yang B, Wang B, Schmitt SE, Wang B, Lucy KA, Ishikawa H, Schuman JS, Smith MA, Wollstein G, Sigal IA. Comparing acute IOP-induced lamina cribrosa deformations premortem and postmortem. Transl Vis Sci Technol. 2022;11(12):1, https://doi.org/10.1167/tvst.11.12.1

Purpose: Lamina cribrosa (LC) deformations caused by elevated intraocular pressure (IOP) are believed to contribute to glaucomatous neuropathy and have therefore been extensively studied, in many conditions, from in vivo to ex vivo. We compare acute IOP-induced global and local LC deformations immediately before (premortem) and after (postmortem) sacrifice by exsanguination.

Methods: The optic nerve heads of three healthy monkeys 12 to 15 years old were imaged with spectral-domain optical coherence tomography under controlled IOP premortem and postmortem. Volume scans were acquired at baseline IOP (8–10 mm Hg) and at 15, 30, and 40 mm Hg IOP. A digital volume correlation technique was used to determine the IOP-induced three-dimensional LC deformations (strains) in regions visible premortem and postmortem.

Results: Both conditions exhibited similar nonlinear relationships between IOP increases and LC deformations. Median effective and shear strains were, on average, over all eyes and pressures, smaller postmortem than premortem, by 14% and 11%, respectively (P's < 0.001). Locally, however, the differences in LC deformation between conditions were variable. Some regions were subjected premortem to triple the strains observed postmortem, and others suffered smaller deformations premortem than postmortem.

Conclusions: Increasing IOP acutely caused nonlinear LC deformations with an overall smaller effect postmortem than premortem. Locally, deformations premortem and postmortem were sometimes substantially different. We suggest that the differences may be due to weakened mechanical support from the unpressurized central retinal vessels postmortem.

Translational Relevance: Additional to the important premortem information, comparison with postmortem provides a unique context essential to understand the translational relevance of all postmortem biomechanics literature.

Introduction

Loss of vision in glaucoma, a leading cause of blindness worldwide, is due to damage to the retinal ganglion cell axons that transmit visual information from the light-sensitive retina to the brain.[1] Damage to these axons is believed to initiate within the lamina cribrosa (LC), a structure within the optic nerve head through which the axons pass to exit the eye on their way to the brain.[1,2] Elevated intraocular pressure (IOP) is a primary risk factor for glaucoma, and the only modifiable one. Nevertheless, the mechanisms by which elevated IOP contributes to neural tissue damage and vision loss are not fully understood. It is widely believed that IOP-induced deformations of the LC play a central role in the process of glaucomatous neuropathy.[2–7]

Due to technical limitations and ethical considerations, many experimental studies on LC biomechanics have been done on ocular tissues ex vivo (after death and enucleation).[7–15] With advances in imaging technologies, especially optical coherence tomography (OCT), there has been an increase in studies of LC biomechanics in vivo.[4,16–22] Current knowledge of LC biomechanics is therefore a mix of lessons learned from a diverse mix in experimental settings, supplemented by analytic and computational modeling.[6,23–31]

It seems reasonable to suspect that there may be important differences in tissue behavior between conditions. Ocular tissues can degrade, swell or dehydrate over time, shrink during preservation, or distort during histologic processing.[32,33] From a biomechanics perspective, enucleated globes are no longer subjected to the forces from intraocular, cerebrospinal, arterial, venous, episcleral, and orbital pressures or from the muscles or eyelid action. There may be stress release from dissection. Some of these differences may be reduced in an ex vivo experiment by attempting to mimic the conditions before enucleation, such as mounting the posterior pole in an inflation chamber.[34,35] Nevertheless, these approaches are unlikely to fully reproduce the complexity of the in vivo conditions, and therefore the potential remains that the specific conditions used for an experiment may have influenced the findings. To the best of our knowledge, the differences in LC biomechanics between in vivo and ex vivo conditions remain largely unknown. This precludes a proper interpretation of the findings in a given condition and an understanding of their implications on other conditions.

Our goal in this study was to compare acute IOP-induced LC deformations immediately before (premortem) and after (postmortem) death. The differences between these two, close, yet fundamentally distinct, conditions will provide information useful to understand differences between other possible experimental conditions. We adopted an experimental approach introduced by our group to image with OCT the posterior pole of healthy monkeys premortem and postmortem while at several controlled IOP levels.[4,36–38] We then analyzed the images to quantify acute IOP-induced LC deformations and identify any differences between premortem and postmortem responses.

Methods

Our general strategy was the following: the optic nerve heads of five eyes from three healthy adult rhesus macaque monkeys were imaged using OCT at various levels of IOP when alive (premortem) and immediately after death (postmortem). A digital volume correlation (DVC) technique was then used to find the local displacements that brought an image acquired at low IOP into coincidence with the one acquired at elevated IOP. From the displacements, we computed the three-dimensional (3D) deformations of the LC caused by the acute increase in IOP, which we then analyzed to determine if there were differences in the LC deformations premortem and postmortem.

A note on terminology: we considered several potential terms before settling on premortem and postmortem. We discarded ex vivo because it implies that the tissues had been removed from the body, which was not the case. We considered before and after death, but there were concerns that these did not seem "scientific," perhaps because they are not in Latin. This was also the reason to discard "alive," "alive condition," and "death condition." Other multiword terms were considered, such as "in situ ex vivo," but we preferred the simplicity of a single term. Accordingly, we opted to use premortem instead of in vivo because it afforded the symmetry of premortem versus postmortem.

Animal Handling and Pressure Setup

All procedures were approved by the University of Pittsburgh's Institutional Animal Care and Use Committee and adhered to both the guidelines established in the National Institutes of Health's Guide for the Care and Use of Laboratory Animals and the Association for Research in Vision and Ophthalmology statement on the use of animals in ophthalmic and vision research.

The details of animal handling and pressure setup (Fig. 1) have been described previously.[4,36] Briefly, the animal was initially sedated with ketamine (20 mg/kg),

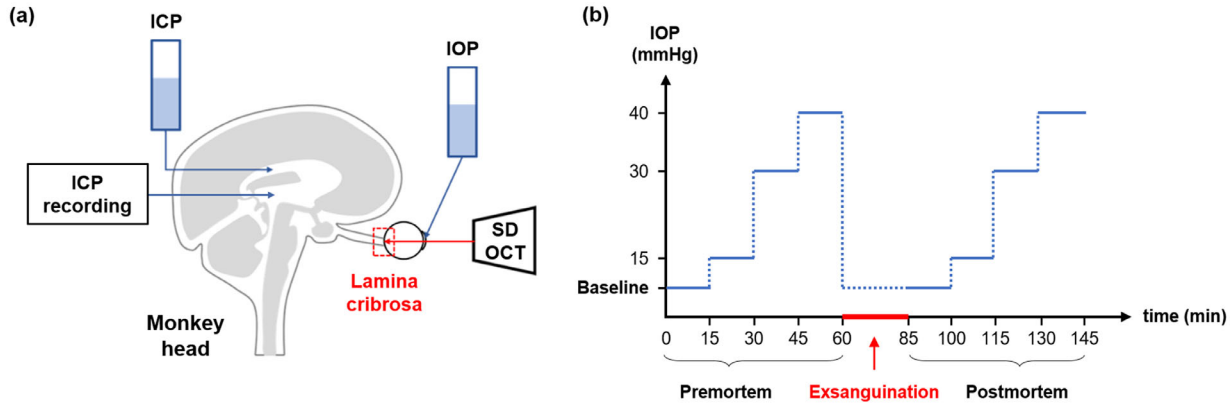

Figure 1. (a) Experimental setup modified from Tran et al.[36] (b) Elevations of IOP in the premortem and postmortem conditions. Baseline IOP was set to 8 mm Hg for M1 and M3 and 10 mm Hg for M2. IOP was then raised stepwise from the baseline to 15, 30, and 40 mm Hg, with each pressure step lasting about 15 minutes: 5-minute "wait" after an IOP elevation and about 10 minutes for the scanning. For M1 and M3, we varied IOP in one eye premortem and the contralateral one postmortem. For M2, we varied IOP in the same eye premortem and postmortem. There was an interval of 25 minutes between the premortem and postmortem conditions. In both conditions, the OCT scans were first acquired at baseline IOP and then at elevated IOPs.

diazepam (1 mg/kg), and atropine (0.04 mg/kg) and was then maintained on isoflurane (1%–3%) for the remainder of the experiment. An arterial line was placed in the animal's carotid or femoral artery, allowing for continuous recording of the intra-arterial pressure. After the arterial line was placed, the animal was put on a ventilator and was given a paralytic intravenously (vecuronium bromide, 2 mL/h) to reduce eye movements. To record and control intracranial pressure (ICP), two small craniotomies were performed to insert a catheter (EDM lumbar catheter; Medtronic, Minneapolis, MN, USA) into the lateral ventricle and a sensor (Precision Pressure Catheter; Raumedic, Mills River, NC, USA) nearby into the parenchyma of the brain. The catheter was connected to a saline reservoir for ease of manipulating ICP (Aqualite 0.9%). IOP was controlled by inserting into the anterior chamber a 27-gauge needle, which was connected to another saline reservoir. The needle was secured to the head at the iris plane. Care was taken to ensure that it did not distort or damage the lens or cornea. To record IOP, an inline transducer was placed between the needle and the saline reservoir (TransStar; Smith Medical, Dublin, OH, USA). M1, M2, and M3 were 12, 15, and 14 years old, respectively. Note that the same machine was used to record the ICP, IOP, and arterial pressure data.

Premortem Condition

For premortem imaging, ICP was set to 9 mm Hg, the normal ICP level in healthy animals.[39,40] IOP was initially set to 8 mm Hg for monkey 1 (M1) and monkey 3 (M3) and 10 mm Hg for monkey 2 (M2). IOP was then raised stepwise from the baseline pressure to 15, 30, and 40 mm Hg, with each pressure step lasting approximately 15 minutes. IOP, ICP, and blood pressure were measured and continuously recorded digitally at a rate of 100 Hz (MPR 1 DATALOGGER; Raumedic).

Exsanguination and Postmortem Condition

Before exsanguination, 3000 to 5000 units of heparin were given intravenously and isoflurane was increased to the upper end of the specified range to ensure deep anesthesia. The intravenous saline drip was also left open during the exsanguination to assist flow. Suction was then added to the arterial line with a vacuum pressure of 584 mm Hg. The valve was periodically closed to obtain a blood pressure reading, and the suction was then continued. Animal death was defined as the moment when there was no longer a heartbeat or a blood pressure reading and no pulsation of blood vessels on the OCT viewer. In the postmortem condition, we controlled and measured IOP only.

Image Acquisition

The animal was placed in a prone position during OCT imaging. The eyes were kept open using a wire speculum. Tropicamide drops (0.5%; Bausch & Lomb, Rochester, NY, USA) were used to dilate the pupils. The cornea was fitted with a rigid gas-permeable contact lens (Boston EO, Boston, MA, USA) to improve image quality and kept hydrated throughout the experiment with artificial tears.

Spectral-domain OCT (Leica, Chicago, IL, USA), with a broadband superluminescent diode light source (Superlum, Dublin, Ireland; $\lambda = 870$ nm, $\Delta\lambda = 200$ nm), was used to acquire 3D volume scans (3 mm $\times$ 3 mm $\times$ 1.92 mm with 400 $\times$ 400 $\times$ 1024 voxels sampling) of the optic nerve head region, focused

on the LC. The voxels of the OCT volumes were therefore 7.5 µm × 7.5 µm × 1.875 µm. In both the premortem and postmortem conditions, these scans were first acquired at baseline IOP and then at progressively elevated IOPs. To reduce potential viscoelastic effects, all scans were acquired at least 5 minutes after a given IOP change.[35] Multiple scans were collected at each IOP level, with various focal depth settings. The scans with the best LC microstructure visualization were selected for analysis.

Image Analysis

Motion Artifact Correction

Motion artifacts in the OCT scans result from breathing and heart rate, as well as the environmental vibration of the OCT device and surgical table. To remove the motion artifacts, a traditional method is to apply a nonrigid affine transformation to the scans.[41] However, this method is aggressive and may erroneously remove the true deformations. To avoid this problem, in this work, we utilized a technique that first registered the scans sequentially based on the optic nerve head structures and then corrected motion artifacts using a causal low-pass filter during the registration.[42] A comparison of the OCT scans before and after the correction of motion artifacts is shown in Figure 2.

Noise Reduction

The speckle-like noise in the OCT scans is an inherent artifact in coherence imaging, which can reduce the image contrast and affect both the axial and lateral resolutions.[43] We applied a 3D median filter on the OCT volume scans for noise reduction.[44] A nonlinear sigmoid transfer function was then used to further improve image contrast.[45] A comparison of the OCT scans before and after the noise reduction is shown in Figure 3.

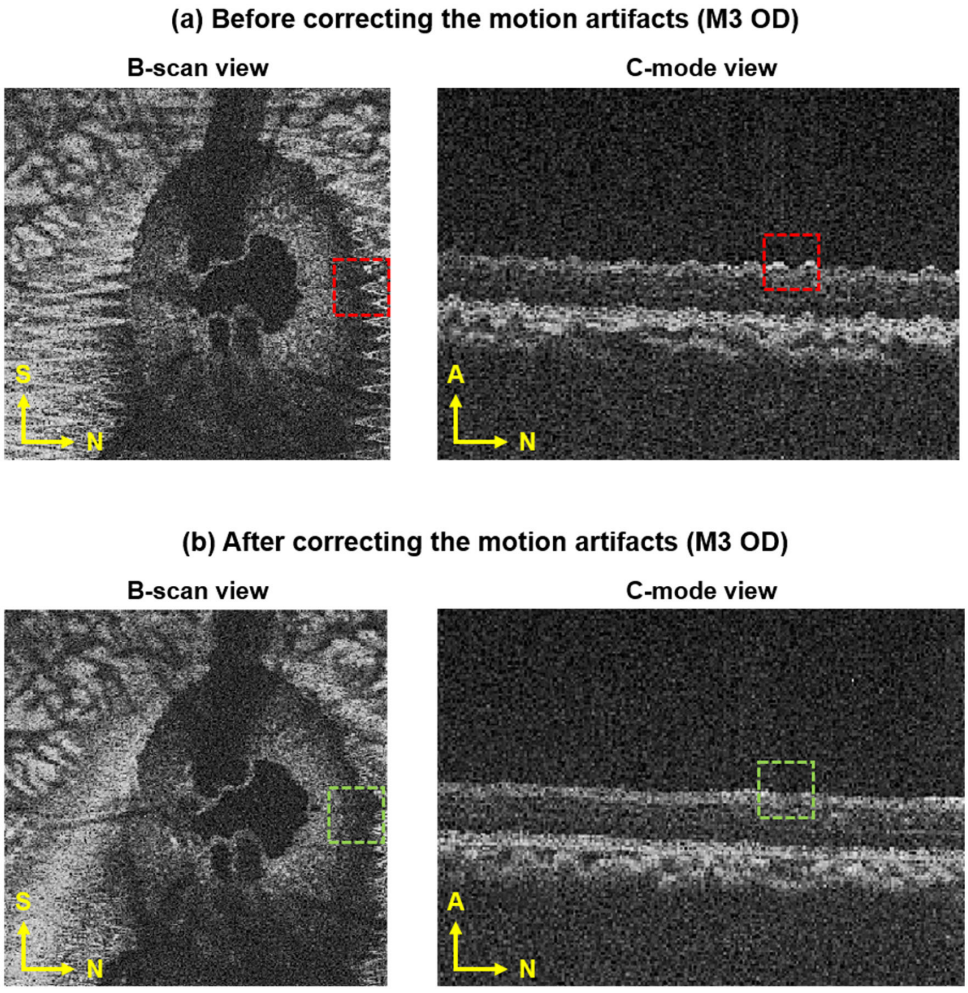

Figure 2. A comparison of OCT scans (a) before and (b) after the correction of motion artifacts. To remove the motion artifacts in OCT scans (*red dotted boxes*), we first registered the scans sequentially based on the optic nerve head structures and then corrected the artifacts using a causal low-pass filter during the registration. Panel (b) shows the efficiency of our method to remove the motion artifacts (*green dotted boxes*). A, anterior; N, nasal; S, superior.

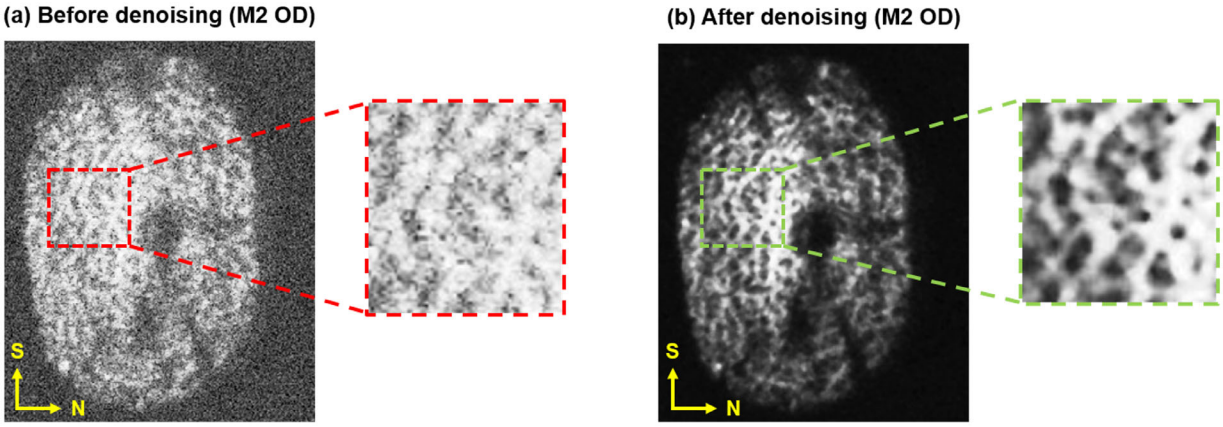

Figure 3. A comparison of OCT scans (a) before and (b) after denoising. We applied a 3D median filter on the OCT volume scans for noise reduction. A nonlinear sigmoid transfer function was then used to further improve the image contrast. Our method was efficient in reducing the speckle-like noise in OCT scans. After denoising, the LC trabecular beams and pores (closeups) were more visible than those before denoising. N, nasal; S, superior.

Digital Volume Correlation

To determine the IOP-induced LC deformations, we used a DVC analysis between multiple OCT scans.[42] For simplicity, the scans were treated as 3D volumetric images. The basic concept of DVC is to establish a mapping between an undeformed volume at baseline IOP (8 mm Hg for M1 and M3, 10 mm Hg for M2) and a deformed one at elevated IOP. The undeformed volume was treated as a baseline volume and then used to compare with each deformed volume. The result of this mapping was a transformation function between two volumes. The transformation function was evaluated by minimizing the error of zero-normalized cross-correlations, which is a numerical metric for finding a similarity.[46] We applied the Nelder–Mead method to minimize the error of zero-normalized cross-correlations.[47,48] The minimization of the correlation values indicates the best matching point in the search region of the deformed volume, and from the matched points, the displacement vector can be calculated. We computed the Green–Lagrange strain tensor from the displacement field at the matched points. The effective strain (a measure of the total deformation including stretch and compression) and the maximum shear strain (a measure of tearing and bending deformations) can be extracted as

$$E_{effective}=\sqrt{\frac{1}{2}\left[(E_1-E_2)^2+(E_1-E_3)^2+(E_2-E_3)^2\right]} \quad (1)$$

$$E_{maxshear}=\frac{1}{2}|E_1-E_3| \quad (2)$$

where E_1, E_2, and E_3 are the principal components of the Green–Lagrange strain tensor. For simplicity, the maximum shear strain is hereafter referred to as shear strain.

Masking

As we have previously reported, exsanguination increases the visibility of the LC.[36] To make a fair comparison of the IOP-induced LC strains between premortem and postmortem conditions, we had to compare only the regions visible in both conditions. For this, the blood vessel shadows in the premortem scans were manually selected and used as a mask on the postmortem scans (Fig. 4). Other low-quality correlations were identified using a statistical z score and removed to ensure that unreliable displacements were not included for computing deformations or considered in the comparison. For monkeys 1 and 3, the image quality postmortem was poor, which substantially reduced the regions of reliable analysis. Thus, for these animals, the comparisons between premortem and postmortem conditions were made with the contralateral eye. This required carefully registering and mirroring the images of the contralateral eye.

Statistical Analysis

We determined whether the IOP-induced LC strains were significantly different between premortem and postmortem conditions using linear mixed-effects models. As a fixed variable, we used the condition premortem or postmortem. The random variables were factors that may affect the sampling population, such as the level of IOP. Our analysis included voxels from the whole lamina for both the premortem and postmortem OCT volume scans. The statistical analy-

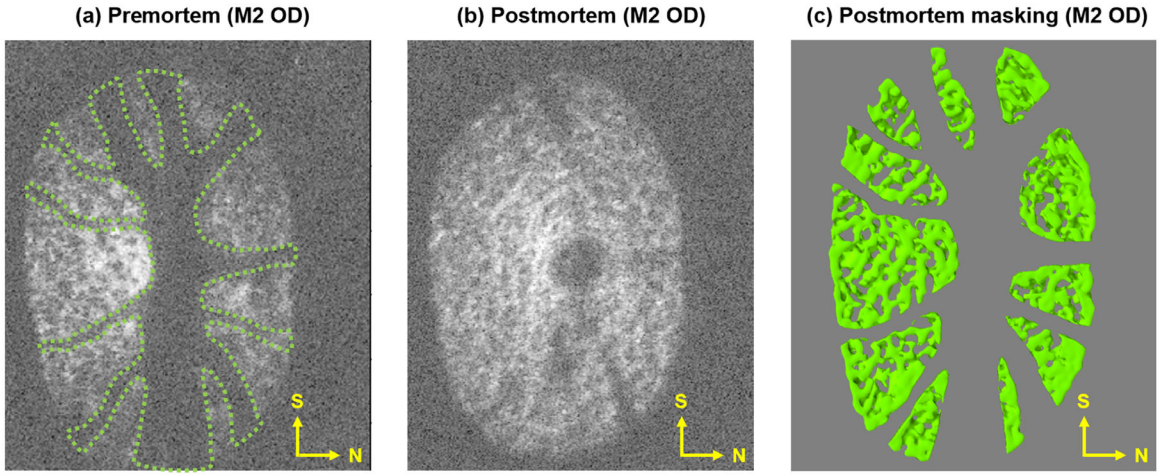

Figure 4. Demonstration of shadow masking. (a) C-mode view of the LC at baseline IOP in the premortem condition. The outline of blood vessel shadows was manually delineated and used to identify the region for comparison. (b) C-mode view of the LC at baseline IOP in the postmortem condition. (c) The same scan in the postmortem condition masked using the outline from the scan in the premortem condition. N, nasal; S, superior.

sis was based on points tracked within the visible LCs. Sample sizes were 2249 for M1, 1731 for M2, and 2221 for M3. We removed the spatial autocorrelation by specifying an exponential spatial correlation structure using the cartesian distance between voxels within each scan volume.[49] We used $\alpha = 0.001$ to establish significance. Statistical analysis was done with R v3.2.2 (R Foundation for Statistical Computing, Vienna, Austria).

Results

In both the premortem and postmortem conditions, our image registration technique performed well to match low and high IOP images (Fig. 5). Before the registration, the differences in images could not be removed by simple translation or rotation. Conversely, after the registration, there was an excellent match

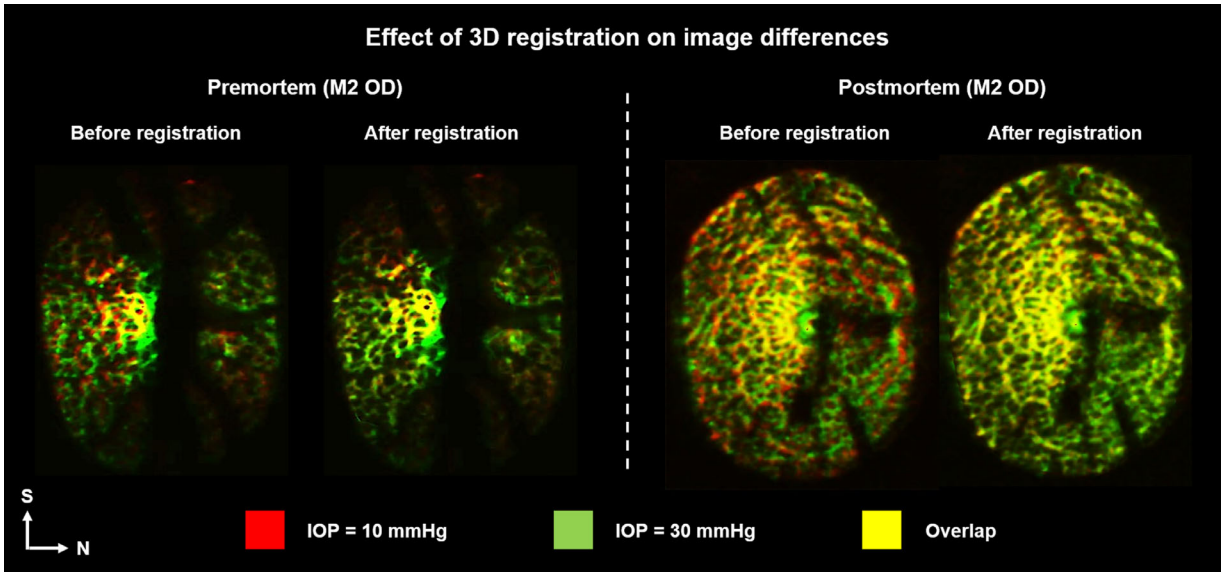

Figure 5. Demonstration of the 3D image registration technique in the premortem (*left*) and postmortem (*right*) conditions. Shown are OCT C-mode view acquired at IOPs of 10 mm Hg (*red*) and 30 mm Hg (*green*) to visualize the differences and overlap (*yellow*). The differences before registration cannot be removed by simple translation or rotation. The 3D registration produced excellent coincidence between the images, without concentrations. The largest differences were due to noise and intensity variations that result in slightly *greenish* or *reddish* regions despite the coincidence of the LC features. N, nasal; S, superior.

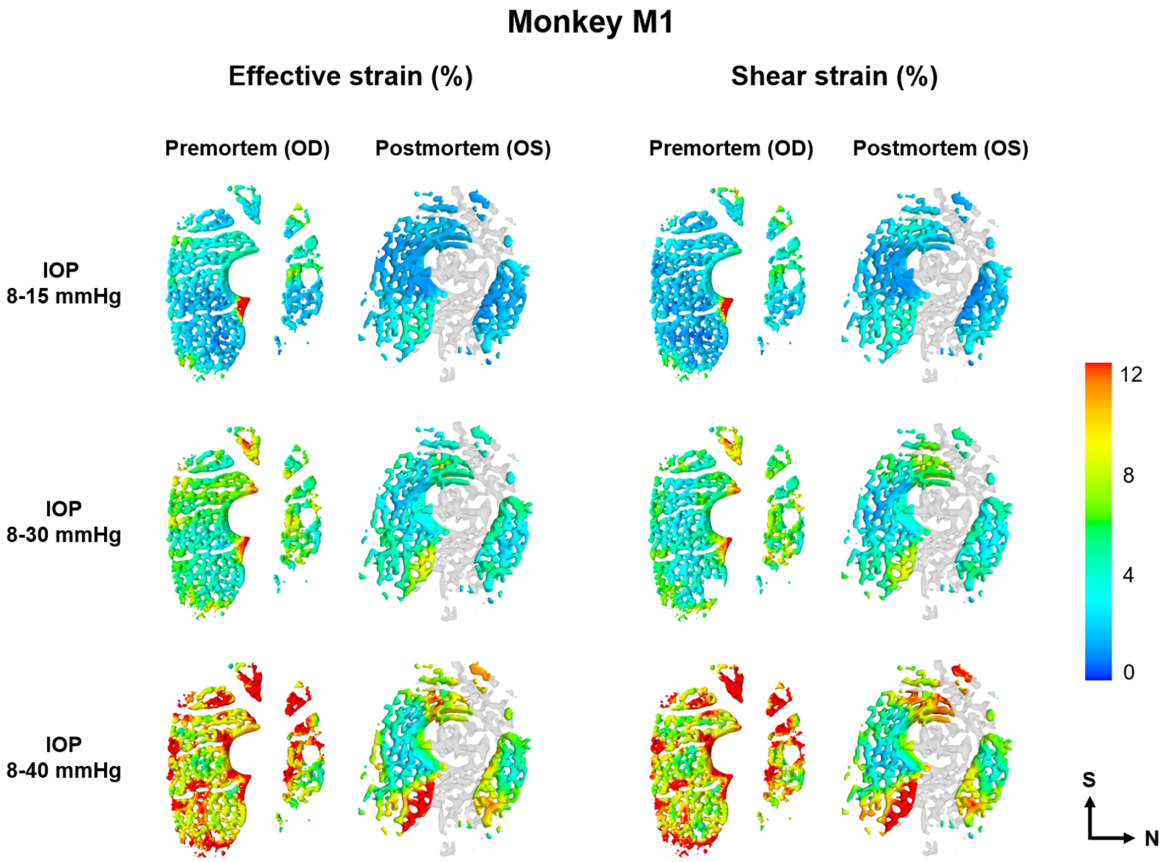

Figure 6. Contour plots of the IOP-induced LC strains of monkey M1 in the premortem and postmortem conditions. *Left two columns*: the effective strain in the premortem and postmortem conditions; *right two columns*: the shear strain in the premortem and postmortem conditions. Rows 1 to 3 correspond to the three levels of IOP elevation (from low to high). The distribution of the effective strain was similar to that of the shear strain, which was highly focal and concentrated in regions as small as a few pores. IOP-induced LC strains were overall smaller postmortem than premortem, but locally, a few locations had larger strains postmortem than premortem. OS images were flipped for ease of comparison. N, nasal; S, superior.

between images with the overlapping regions of lamina beams and pores. The minor differences in images are due to the noise and intensity variations that result in the slightly greenish or reddish regions despite the coincidence of the LC features.

The LC strains increased with IOP in both the premortem and postmortem conditions (Figs. 6–8). IOP-induced LC strains were highly focal and concentrated in regions as small as a few pores. Maps of the image differences before and after registration demonstrate that this was not a registration artifact (Fig. 5). Overall, IOP-induced LC strains were smaller postmortem than premortem. Locally, some regions were subjected premortem to triple the strains observed postmortem, whereas a few locations had larger strains postmortem than premortem (Fig. 9).

Figure 10 shows a quantitative comparison of the IOP-induced LC strains between premortem and postmortem conditions. On average, over the three monkeys, the effective and shear strains decreased by 14.4% and 11.0%, respectively, in the postmortem condition relative to those in the premortem condition. The largest decreases were in M3 when IOP increased from 8 to 15 mm Hg, in which the effective and shear strains decreased by 23.3% and 16.6%, respectively ($P < 0.001$). Compared with the premortem condition, IOP-induced LC strains in the postmortem condition were less variable.

The LC median strains increased nonlinearly with IOP in both the premortem and postmortem conditions (Fig. 11). For example, when IOP increased from 15 to 30 mm Hg, the effective strain increased by an average of 101.6% and 123.1%, respectively, in the premortem and postmortem conditions. In comparison, when IOP increased from 30 to 40 mm Hg, the effective strain only increased by an average of 32.5% and 35.4%, respectively, in both conditions.

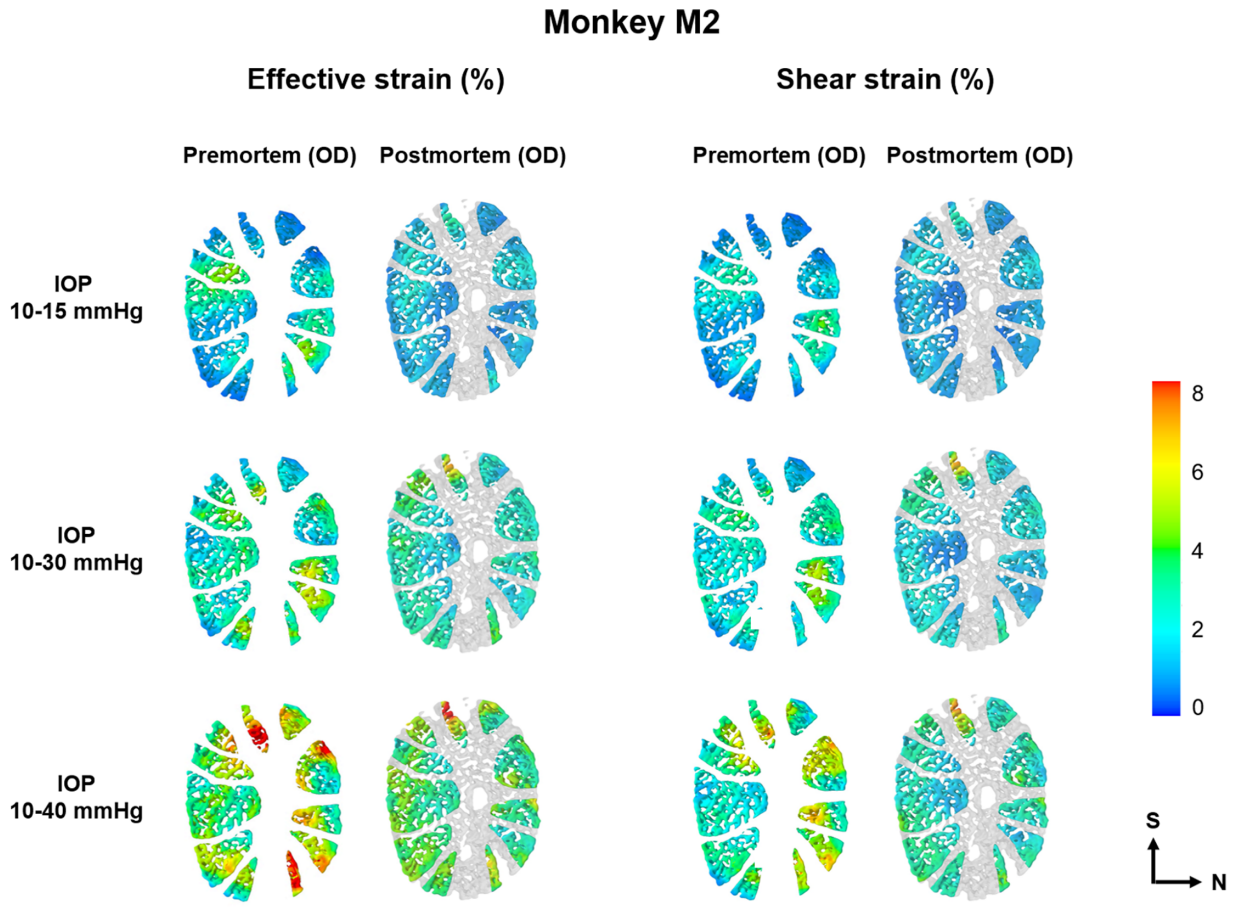

Figure 7. Contour plots of the IOP-induced LC strains of monkey M2 in the premortem and postmortem conditions. *Left two columns*: the effective strain in the premortem and postmortem conditions; *right two columns*: the shear strain in the premortem and postmortem conditions. Rows 1 to 3 correspond to the three levels of IOP elevation (from low to high). Similar to the observations of M1 (Fig. 6), IOP-induced LC strains were overall smaller postmortem than premortem, but locally, a few locations had larger strains postmortem than premortem. Note that the color scale of these plots is different from that of Figures 6 and 8. The range was selected to help discern details of the patterns. N, nasal; S, superior.

Discussion

Our goal was to compare the acute IOP-induced 3D LC deformations immediately before and after death. Overall, IOP-induced LC deformations were smaller postmortem than premortem, but the trends in the nonlinear relationships with IOP were similar. Locally, deformations premortem and postmortem were sometimes substantially different, with some regions suffering much smaller and some larger postmortem deformations than premortem.

This study provides important information that we have not found elsewhere on the differences between the effects of IOP on the LC premortem and postmortem. We postulate that the decreased IOP-induced LC strains postmortem can be explained by weakened mechanical support from the central retinal vessel postmortem due to the loss of hydraulic stiffness after exsanguination (Fig. 12). Without the support from the vessel, the central LC displaces posteriorly, even at normal IOP. From this condition, the increases in IOP cause deformations that are smaller postmortem in the central LC and larger in the peripheral LC. This interpretation is supported by a direct visualization of OCTs overlaid on each other (Fig. 13).

Our finding of the decreased IOP-induced LC strains postmortem than premortem is consistent with recent measurements in human, monkey, and porcine eyes. For example, premortem studies on human[21] and monkey[22] eyes reported that strains in the LC could reach 10% to 20% as IOP increased by a range of 10 to 23 mm Hg. In comparison, postmortem studies on human[12,13,15] and porcine[14] eyes generally measured the LC strains less than 10% as IOP increased by a range of 10 to 40 mm Hg. The differences in the IOP-induced LC strains between premortem and postmortem conditions are likely smaller than those

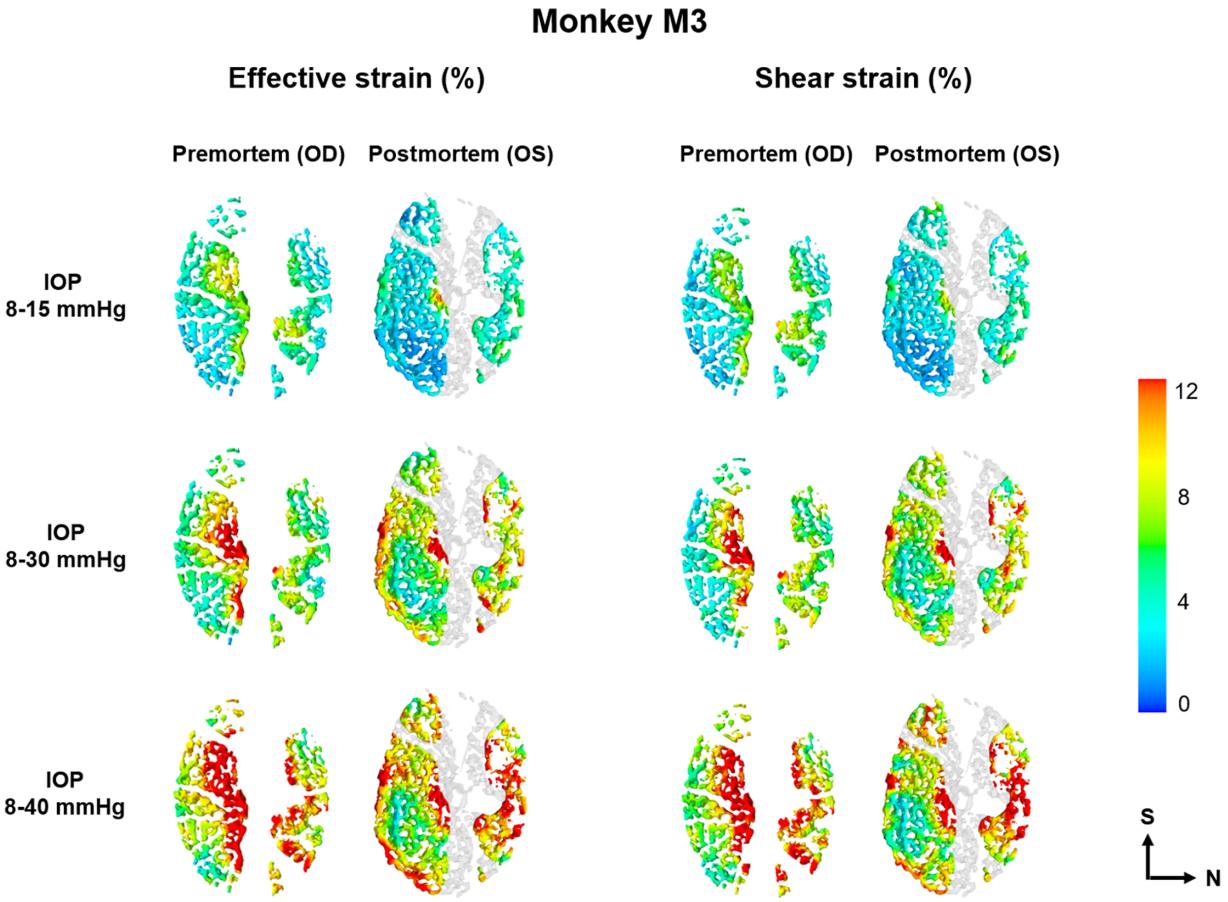

Figure 8. Contour plots of the IOP-induced LC strains of monkey M3 in the premortem and postmortem conditions. *Left two columns*: the effective strain in the premortem and postmortem conditions; *right two columns*: the shear strain in the premortem and postmortem conditions. Rows 1 to 3 correspond to the three levels of IOP elevation (from low to high). Similar to the observations of M1 (Fig. 6), the IOP-induced LC strains were overall smaller postmortem than premortem, but locally, a few locations had larger strains postmortem than premortem. N, nasal; S, superior.

between premortem and ex vivo studies done after the eye has been enucleated and dissected. Enucleated eyes have more differences with the premortem condition that might affect the regional mechanical response, including loss of orbital support, changes in choroidal volume,[50] and longer times between death and testing, sometimes of multiple days.[51] Thus, our measurements also provide a lower boundary estimate of the combined effects of sacrifice and enucleation.

The observed nonlinear relationship between IOP and LC median strains in both conditions is likely primarily determined by tissue property nonlinearities, which are, in turn, determined in large part by collagen fiber undulations, or crimp.[52–55] Using polarized light microscopy, we have reported microstructural crimp of collagen fibers in the LC and sclera at normal IOPs.[53] The crimp gradually vanished as IOP increased, contributing to the local stiffening of the tissue.[52] This process is called collagen fiber recruitment, which is well recognized in other tissues, like tendons and ligaments.[56–58] It is important to acknowledge that, while crimp plays a central role in soft tissue mechanics, it is not the only factor affecting the mechanical properties. Several other factors also affect tissue stiffness and the response to load, including, but not limited to, fiber type, composition, thickness, alignment and slip conditions, proteoglycan and elastin content and distribution, the amount and type of cross-linking between fibers, and the presence and characteristics of blood vessels within.[56,59–64]

A key strength of our study is that the IOP-induced LC strains were measured in 3D by DVC premortem and postmortem. The LC is intrinsically a 3D structure, and capturing its deformations in 3D renders more robust measurements and a better representation of the actual deformations than a two-dimensional approximation. To improve the accuracy of our DVC

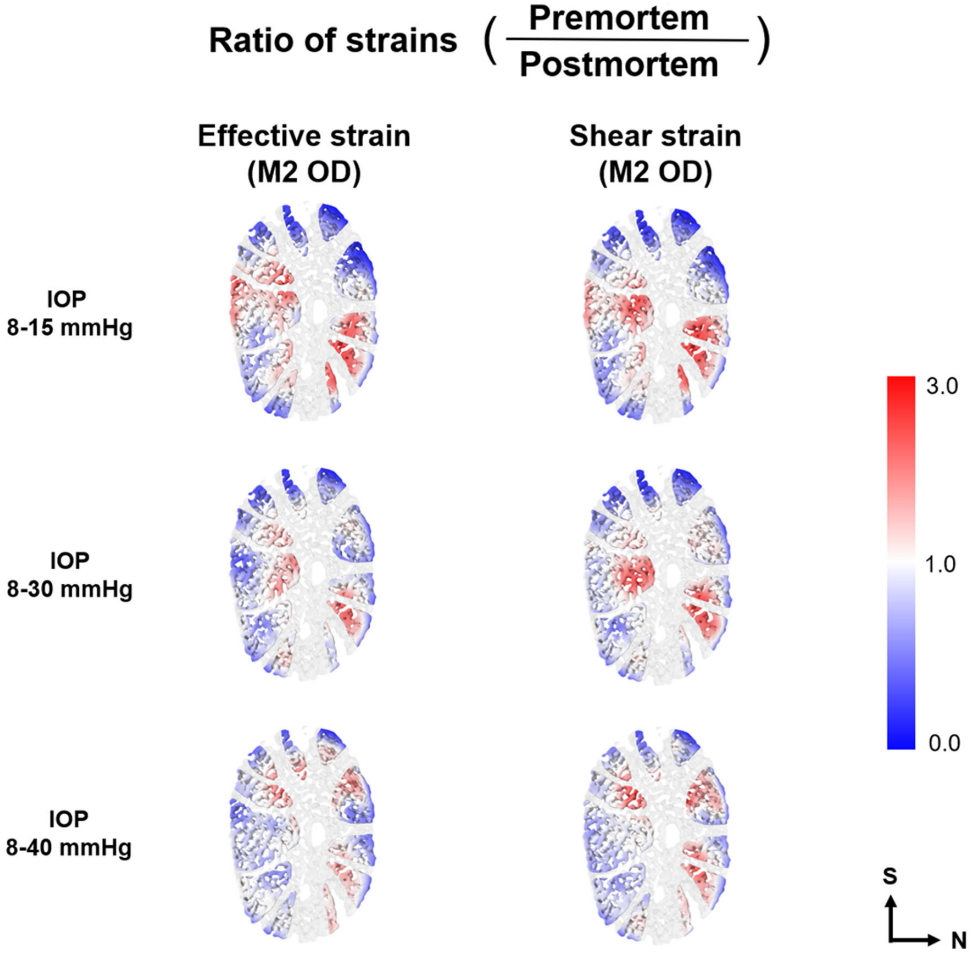

Figure 9. Contour plots of the ratio of IOP-induced LC strains between premortem and postmortem conditions (M2 OD). *Left column*: the effective strain; *right column*: the shear strain. Rows 1 to 3 correspond to the three levels of IOP elevation (from low to high). Larger strains in the premortem condition are shown in *red* and smaller strains in *blue*. Some regions were subjected premortem to triple the strains than postmortem (*red*). A few locations had larger strains postmortem than premortem (*blue*). N, nasal; S, superior.

measurements, we corrected the motion artifacts and reduced the speckle-like noise in OCT scans before image registration. We also examined the correlation coefficients after the DVC measurements (Fig. 14). We then verified our DVC measurements by recovering the undeformed scans from applying the calculated displacement vectors to the deformed ones. Measuring the LC deformations at multiple levels of IOP allowed us to track the continuous deformation of the LC and to capture the nonlinear relationship between IOP and LC strains. The combination of OCT imaging and DVC analysis can be further used to track changes, acute or chronic. This could prove powerful to characterize the patterns of damage and causes underlying susceptibility to pathology in eyes with chronic elevated IOP.

Another strength of our study was the correction for spatial autocorrelation done in the statistical analysis. Autocorrelations that remain uncorrected or not accounted for can spuriously increase the confidence in results. We would like to give credit to Fazio et al.[49] for bringing to our attention this important yet extremely uncommon step in the analysis.

It is also important to consider the limitations of our methods when interpreting the results. First, the cornea was fitted with a contact lens to improve image quality. Although the benefits of using the contact lens for imaging make it worthwhile, it may have affected the response of the globe to IOP and the biomechanics of the posterior pole.[65] However, the lens was present in both premortem and postmortem conditions, so the effects on the comparative results observed in this work are expected to be minor and unlikely to affect the conclusions overall.

Second, due to the substantial shadowing from the vasculature in the premortem scans, the differences in the IOP-induced LC strains between premortem and

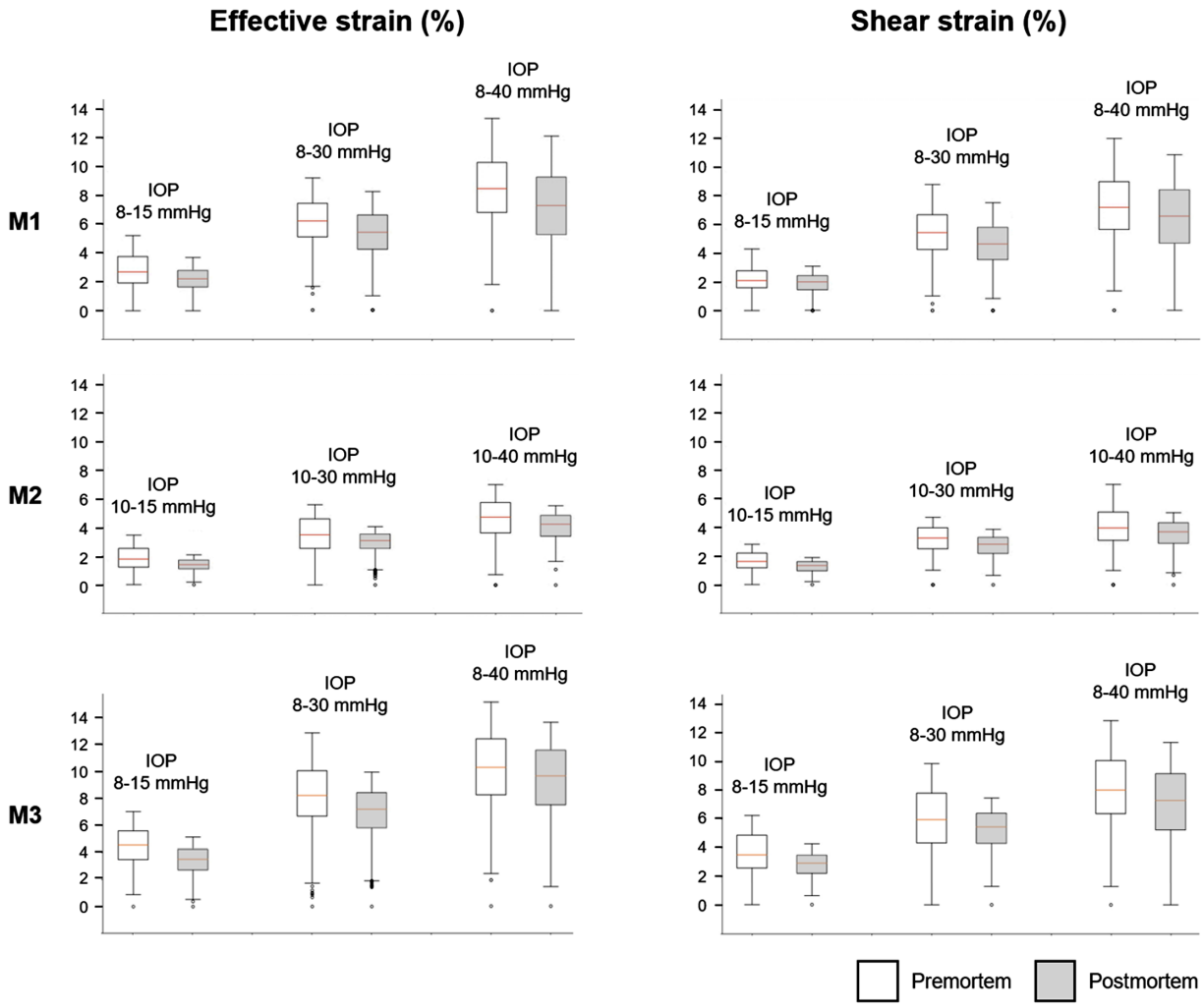

Figure 10. Boxplots of IOP-induced LC strains in the premortem and postmortem conditions. *Left column*: the effective strain; *right column*: the shear strain. Rows 1 to 3 correspond to the strain measurements in M1 to M3. Overall, IOP-induced LC strains postmortem were smaller and less variable than premortem. On average, the effective and shear strains decreased by 14.4% and 11.0%, respectively, in the postmortem condition relative to those in the premortem condition. The largest decreases were in M3 when IOP increased from 8 to 15 mm Hg, in which the effective and shear strains decreased by 23.3% and 16.6%, respectively ($P < 0.001$).

postmortem conditions were determined by comparing only measurements from the same visible regions.[36] Several studies have suggested that the IOP-induced LC strains near the central retinal vessels (e.g., within the shadow regions) are smaller than further away.[12,28,29,31] These are based on a similar rationale of the premortem vasculature providing structural support to the adjacent tissues. Thus, although our method reduces the region available for analysis, it is necessary to avoid a potentially crucial bias.

Third, a reader may wonder if premortem IOP variations could have affected the globe in a way that would affect the LC deformations measured postmortem. We are confident that this is not the case. We selected the IOP levels to represent a wide range from low, but physiologic, to high, but still realistic. Nevertheless, these IOP levels are well within the range of IOPs that happens during eye rubbing[66] and well below those expected to cause acute damage to the eye.[67] Further, only for one of the animals (M2) did we analyze IOP variations in the same eye. In the other two animals (M1 and M3), we made our measurements in different eyes premortem and postmortem. This may help explain the larger difference in the IOP-induced LC strains between premortem and postmortem conditions for M1 and M3 than that for M2. However, this should not affect our conclusions, as previous studies in monkeys using histomorphometry have demonstrated that the contralateral eyes had much more similar deformations than unrelated eyes.[11] While the assumption that the contralateral eyes have similar responses to IOP may apply to monkey eyes, it is still

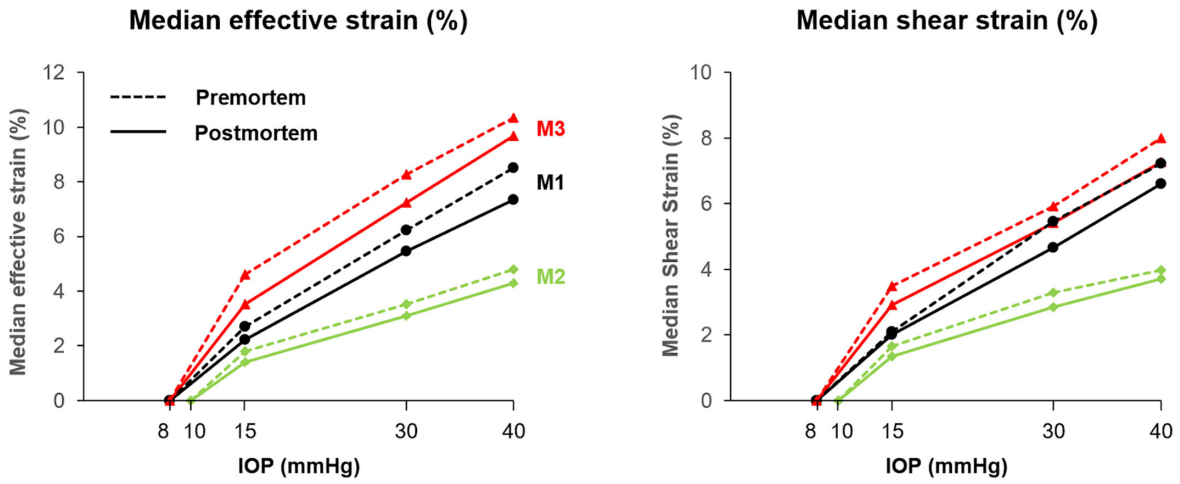

Figure 11. Comparison of IOP-induced LC median strains in the premortem (*dashed line*) and postmortem (*solid line*) conditions of M1 to M3. *Left*: the median effective strain; *right*: the median shear strain. For all the three monkeys, the median effective and shear strains increased nonlinearly with IOP in both the premortem and postmortem conditions. Although the values were different, the trends were similar premortem and postmortem.

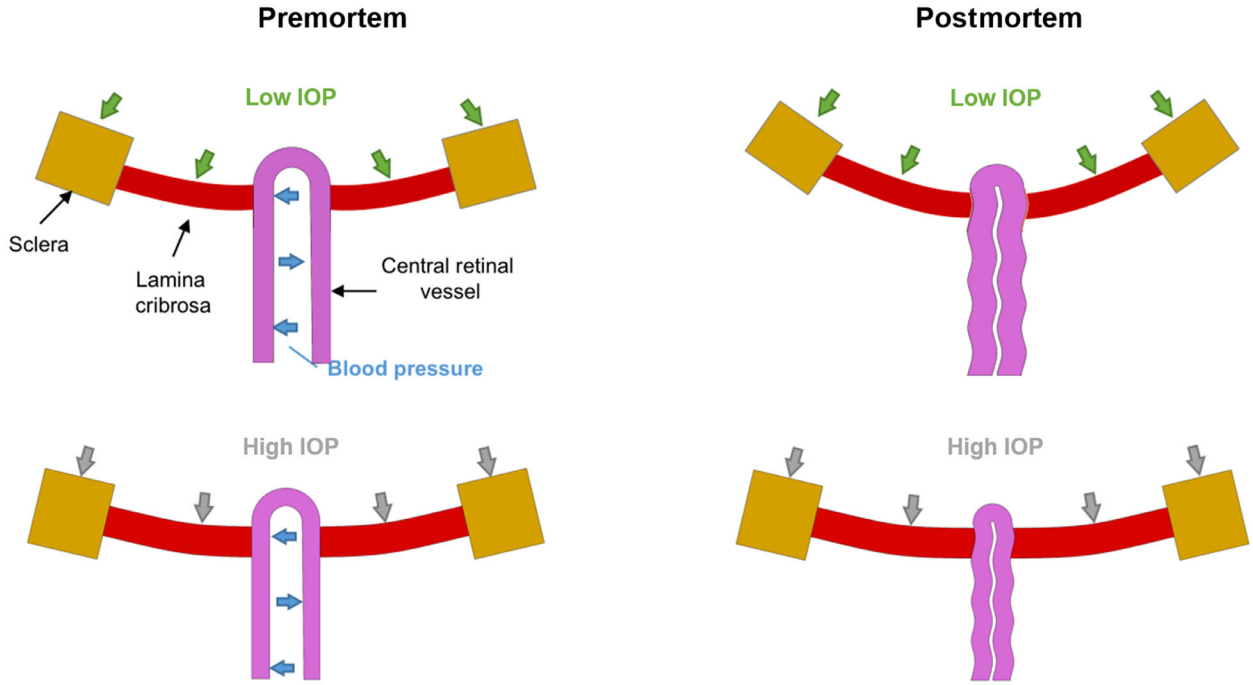

Figure 12. Schematic representation of how the central retinal vessel influences the IOP-induced LC deformations in the premortem and postmortem conditions. In this framework, in the premortem condition, the central retinal vessel acts like a tent pole to support the central region of the LC.[28,68] As IOP increases, the direct effects of IOP "push" the LC posteriorly, and the indirect effects deform the sclera, expanding the canal, which in turn "pull" the LC taut from the sides.[69] After exsanguination, even at normal IOP, the vessel collapses due to the loss of blood pressure.[36] Without the support of vessel, the central region of the LC in the postmortem condition also moves posteriorly relative to the premortem condition. As IOP increases, further posterior displacement of the LC is limited, resulting in the decreased LC strains in the postmortem condition.

unclear how well it holds for human eyes. Some studies of enucleated eyes have reported good contralateral similarity in acute response to IOP,[13] whereas others found a somewhat low contralateral similarity.[12] Overall, we acknowledge that our comparisons for M1 and M3 rest on the assumption that contralateral eyes of an animal have similar acute responses to IOP.

Fourth, we did not manipulate ICP in the postmortem condition. As a result, the translam-

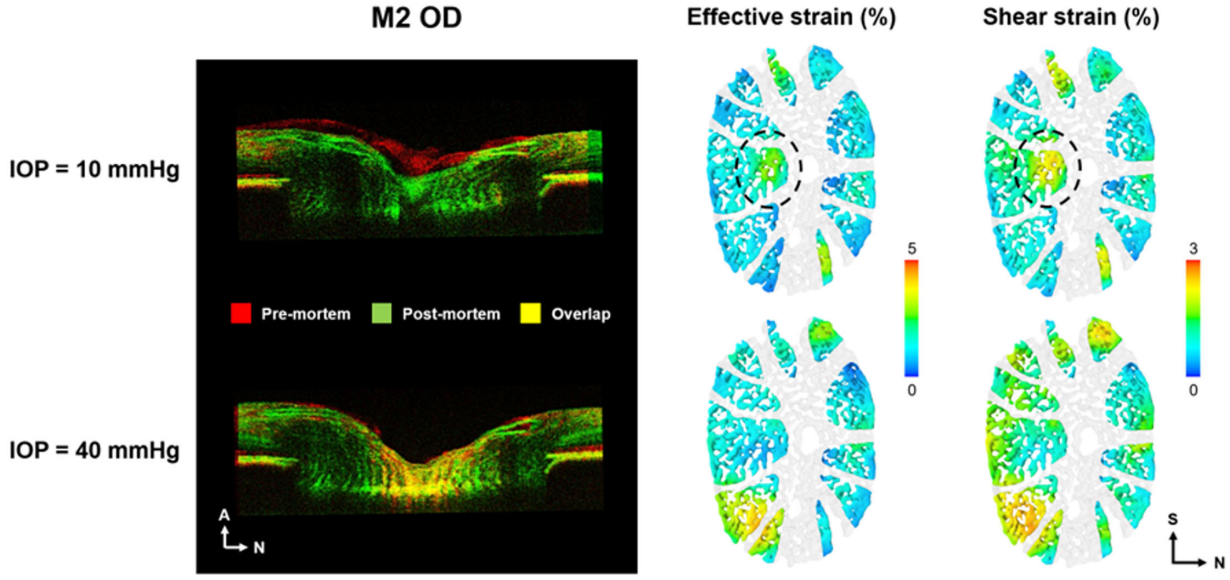

Figure 13. Comparison of the optic nerve head between premortem and postmortem conditions. Shown on the *left* are OCT B-scans for M2 OD acquired at IOPs of 10 mm Hg (*top*) and 40 mm Hg (*bottom*). The premortem scan is shown in *red*, and the postmortem scan is shown in *green*, with *yellow* representing overlap. Shown on the *right* are the effective and shear strains of the LC calculated by DVC between pre- and postmortem conditions. At baseline IOP (10 mm Hg), the central LC in the postmortem condition was displaced more posteriorly relative to the premortem condition. This is consistent with the DVC measurements showing larger strains in the central region of the LC (as indicated by the *dashed circle*). A potential explanation is that, in the premortem condition, the central retinal vessels are under hydraulic stiffening from blood pressure and thus provide support to the adjacent tissues. After exsanguination, the vessels collapse due to the loss of blood pressure, resulting in the tissues being displaced posteriorly. It is also interesting that the large displacements were accompanied by LC strains comparable to those caused by fairly large changes in IOP. As IOP increases to 40 mm Hg (*bottom*), further posterior displacement of the LC is limited in the postmortem condition, resulting in smaller LC strains postmortem than premortem. A, anterior; N, nasal; S, superior.

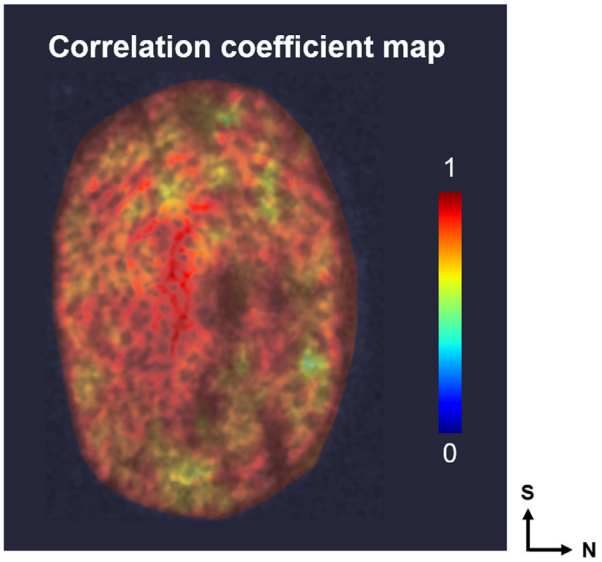

Figure 14. An example of correlation coefficient map overlaid on the OCT image (M2 OD postmortem). The high correlations indicate a robust DVC analysis. Note that the correlation coefficients are discrete. We interpolated the coefficient values to generate the contour plot.

inar pressure difference (IOP – ICP) postmortem may be different from that premortem. In addition, the extraorbital pressure may change, and the support from the extraocular muscles may be different postmortem. Therefore, the changes in strains in the LC may be a combination of lack of blood pressure, change in ICP and extraorbital pressure, and altered muscle load. How exactly these changes contribute to the decreased LC strains postmortem remains unclear and should be clarified in future studies.

Fifth, although we waited after pressure changes and between conditions to allow the system and tissues to stabilize (Fig. 1), the interval necessary to fully converge remains unknown. Similarly, it is possible that in eyes tested more than once (M2), the first test affected the second one. There were constraints on the choice of interval length. On one hand, longer intervals after pressure changes and between conditions would help reduce potential effects of the transitions. On the other hand, longer experiments may adversely affect image quality. The intervals chosen were selected based on the literature and our own preliminary work to balance these constraints.

In the study, we compared the IOP-induced LC deformations premortem and postmortem in five eyes of three monkeys, and the comparison results were consistent through the eyes we studied. It is worth reminding the reader that the experiment and analysis were not designed to determine whether our observations in these monkey eyes will extend to other eyes or monkeys. This cannot be determined from the small set of eyes we studied. The goal of our analysis was to obtain a robust set of findings for this particular set of eyes. Additional studies with more eyes and animals are necessary to apply our findings to the general population.

In summary, we have provided novel measurements of the LC deformations resulting from acute IOP increases immediately after death by exsanguination. We also measured the effects of IOP, allowing for a direct premortem versus postmortem comparison. Overall, the acute IOP-induced LC deformations were smaller postmortem than premortem, but the trends in the nonlinear relationship with IOP were similar. Locally, deformations premortem and postmortem can be substantially different, with some regions being much smaller and some larger postmortem than premortem. Our results are expected to help improve the fundamental understanding of how LC biomechanics premortem and postmortem relate to one another and how they depend on blood pressure.

Acknowledgments

The authors thank Huong Tran for help throughout the project.

Supported in part by National Institutes of Health (Bethesda, MD) R01-EY013178, R01-EY023966, R01-EY025011, R01-EY022928, R01-EY028662, R01-EY031708, P30-EY008098, and T32-EY017271; the Eye and Ear Foundation (Pittsburgh, PA); Glaucoma Research Foundation Shaffer Grant; and Research to Prevent Blindness (support to the Department of Ophthalmology and a Stein Innovation Award to IAS).

Disclosure: **J. Wei**, was at the University of Pittsburgh when he contributed to this work; **Y. Hua**, None; **B. Yang**, None; **B. Wang**, None; **S.E. Schmitt**, None; **B. Wang**, None; **K.A. Lucy**, None; **H. Ishikawa**, None; **J.S. Schuman**, Zeiss (F), Carl Zeiss Meditec (C), Opticient (C); **M.A. Smith**, None; **G. Wollstein**, None; **I.A. Sigal**, None

* JW and YH contributed equally to this study. Both are equivalent authors.

References

1. Quigley HA. Glaucoma. *Lancet*. 2011;377:1367–1377.
2. Burgoyne CF. A biomechanical paradigm for axonal insult within the optic nerve head in aging and glaucoma. *Exp Eye Res*. 2011;93:120–132.
3. Sigal IA. Interactions between geometry and mechanical properties on the optic nerve head. *Invest Ophthalmol Vis Sci*. 2009;50:2785–2795.
4. Wang B, Tran H, Smith MA, et al. In-vivo effects of intraocular and intracranial pressures on the lamina cribrosa microstructure. *PLoS One*. 2017;12:e0188302.
5. Quigley HA. Reappraisal of the mechanisms of glaucomatous optic nerve damage. *Eye*. 1987;1:318–322.
6. Zhang L, Albon J, Jones H, et al. Collagen microstructural factors influencing optic nerve head biomechanics. *Invest Ophthalmol Vis Sci*. 2015;56:2031–2042.
7. Coudrillier B, Campbell IC, Read AT, et al. Effects of peripapillary scleral stiffening on the deformation of the lamina cribrosa. *Invest Ophthalmol Vis Sci*. 2016;57:2666–2677.
8. Jones H, Girard M, White N, et al. Quantitative analysis of three-dimensional fibrillar collagen microstructure within the normal, aged and glaucomatous human optic nerve head. *J R Soc Interface*. 2015;12:20150066.
9. Whitford C, Joda A, Jones S, Bao F, Rama P, Elsheikh A. Ex vivo testing of intact eye globes under inflation conditions to determine regional variation of mechanical stiffness. *Eye Vis*. 2016;3:21.
10. Voorhees AP, Ho LC, Jan N-J, et al. Whole-globe biomechanics using high-field MRI. *Exp Eye Res*. 2017;160:85–95.
11. Yang H, Downs JC, Sigal IA, Roberts MD, Thompson H, Burgoyne CF. Deformation of the normal monkey optic nerve head connective tissue after acute IOP elevation within 3-D histomorphometric reconstructions. *Invest Ophthalmol Vis Sci*. 2009;50:5785–5799.
12. Sigal IA, Grimm JL, Jan NJ, Reid K, Minckler DS, Brown DJ. Eye-specific IOP-induced displacements and deformations of human lamina cribrosa. *Invest Ophthalmol Vis Sci*. 2014;55:1–15.

13. Midgett DE, Pease ME, Jefferys JL, et al. The pressure-induced deformation response of the human lamina cribrosa: analysis of regional variations. *Acta Biomaterial*. 2017;53:123–139.
14. Coudrillier B, Geraldes DM, Vo N, et al. A novel micro-computed tomography (μCT) method to measure IOP-induced deformation of the Lamina Cribrosa (LC). *Invest Ophthalmol Vis Sci*. 2015;56:6149–6149.
15. Pavlatos E, Perez BC, Morris HJ, et al. Three-dimensional strains in human posterior sclera using ultrasound speckle tracking. *J Biomech Eng*. 2016;138:021015.
16. Wang B, Nevins JE, Nadler Z, et al. In vivo lamina cribrosa micro-architecture in healthy and glaucomatous eyes as assessed by optical coherence tomography. *Invest Ophthalmol Vis Sci*. 2013;54:8270–8274.
17. Girard MJ, Strouthidis NG, Desjardins A, Mari JM, Ethier CR. In vivo optic nerve head biomechanics: performance testing of a three-dimensional tracking algorithm. *J R Soc Interface*. 2013;10:20130459.
18. Kim YK, Ha A, Song YJ, et al. Valsalva maneuver-induced changes in anterior lamina cribrosa surface DEPTH: a comparison between normal and glaucomatous eyes. *J Glaucoma*. 2017;26:866–874.
19. Fazio MA, Johnstone JK, Smith B, Wang L, Girkin CA. Displacement of the lamina cribrosa in response to acute intraocular pressure elevation in normal individuals of African and European descent. *Invest Ophthalmol Vis Sci*. 2016;57:3331–3339.
20. Wu Z, Lin C, Crowther M, Mak H, Yu M, Leung CK-S. Impact of rates of change of lamina cribrosa and optic nerve head surface depths on visual field progression in glaucoma. *Invest Ophthalmol Vis Sci*. 2017;58:1825–1833.
21. Girard MJ, Beotra MR, Chin KS, et al. In vivo 3-dimensional strain mapping of the optic nerve head following intraocular pressure lowering by trabeculectomy. *Ophthalmology*. 2016;123:1190–1200.
22. Tran H, Grimm J, Wang B, et al. Mapping in-vivo optic nerve head strains caused by intraocular and intracranial pressures. *Proc SPIE Int Soc Opt Eng* 2017;10067:100670B.
23. Voorhees AP, Jan NJ, Sigal IA. Effects of collagen microstructure and material properties on the deformation of the neural tissues of the lamina cribrosa. *Acta Biomaterial*. 2017;58:278–290.
24. Voorhees AP, Jan NJ, Austin ME, et al. Lamina cribrosa pore shape and size as predictors of neural tissue mechanical insult. *Invest Ophthalmol Vis Sci*. 2017;58:5336–5346.
25. Voorhees AP, Jan N-J, Hua Y, Yang B, Sigal IA. Peripapillary sclera architecture revisited: a tangential fiber model and its biomechanical implications. *Acta Biomaterial*. 2018;79:113–122.
26. Voorhees AP, Hua Y, Brazile BL, et al. So-called lamina cribrosa defects may mitigate IOP-induced neural tissue insult. *Invest Ophthalmol Vis Sci*. 2020;61:15.
27. Hua Y, Voorhees AP, Jan N-J, et al. Role of radially aligned scleral collagen fibers in optic nerve head biomechanics. *Exp Eye Res*. 2020;199:108188.
28. Hua Y, Voorhees AP, Sigal IA. Cerebrospinal fluid pressure: revisiting factors influencing optic nerve head biomechanics. *Invest Ophthalmol Vis Sci*. 2018;59:154–165.
29. Hua Y, Tong J, Ghate D, Kedar S, Gu L. Intracranial pressure influences the behavior of the optic nerve head. *J Biomech Eng*. 2017;139:031003.
30. Grytz R, Meschke G, Jonas JB. The collagen fibril architecture in the lamina cribrosa and peripapillary sclera predicted by a computational remodeling approach. *Biomech Model Mechanobiol*. 2011;10:371–382.
31. Feola AJ, Myers JG, Raykin J, et al. Finite element modeling of factors influencing optic nerve head deformation due to intracranial pressure. *Invest Ophthalmol Vis Sci*. 2016;57:1901–1911.
32. Tran H, Jan N-J, Hu D, et al. Formalin fixation and cryosectioning cause only minimal changes in shape or size of ocular tissues. *Sci Rep*. 2017;7:1–11.
33. Abramson DH, Schefler AC, Almeida D, Folberg R. Optic nerve tissue shrinkage during pathologic processing after enucleation for retinoblastoma. *Arch Ophthalmol*. 2003;121:73–75.
34. Feola AJ, Coudrillier B, Mulvihill J, et al. Deformation of the lamina cribrosa and optic nerve due to changes in cerebrospinal fluid pressure. *Invest Ophthalmol Vis Sci*. 2017;58:2070–2078.
35. Sigal IA, Flanagan JG, Tertinegg I, Ethier CR. Reconstruction of human optic nerve heads for finite element modeling. *Technol Health Care*. 2005;13:313–329.
36. Tran H, Wallace J, Zhu Z, et al. Seeing the hidden lamina: effects of exsanguination on the optic nerve head. *Invest Ophthalmol Vis Sci*. 2018;59:2564–2575.
37. Nadler Z, Wang B, Schuman JS, et al. In vivo three-dimensional characterization of the healthy human lamina cribrosa with adaptive optics spectral-

domain optical coherence tomography. *Invest Ophthalmol Vis Sci*. 2014;55:6459–6466.
38. Zhu Z, Waxman S, Wang B, et al. Interplay between intraocular and intracranial pressure effects on the optic nerve head in vivo. *Exp Eye Res*. 2021;213:108809.
39. Jonas JB, Yang D, Wang N. Intracranial pressure and glaucoma. *J Glaucoma*. 2013;22: S13–S14.
40. Ren R, Jonas JB, Tian G, et al. Cerebrospinal fluid pressure in glaucoma: a prospective study. *Ophthalmology*. 2010;117:259–266.
41. Ricco S, Chen M, Ishikawa H, Wollstein G, Schuman J. Correcting motion artifacts in retinal spectral domain optical coherence tomography via image registration. *Med Image Comput Comput Assist Interv*. 2009;12(pt 1):100–107.
42. Wei J, Yang B, Voorhees AP, et al. Measuring in-vivo and in-situ ex-vivo the 3D deformation of the lamina cribrosa microstructure under elevated intraocular pressure. *Proc SPIE*. 2018;10496:1049611.
43. Szkulmowski M, Gorczynska I, Szlag D, Sylwestrzak M, Kowalczyk A, Wojtkowski M. Efficient reduction of speckle noise in optical coherence tomography. *Optics Express*. 2012;20:1337–1359.
44. Ali M, Parlapalli R. *Signal Processing Overview of Optical Coherence Tomography Systems for Medical Imaging*. Texas Instruments. Dallas, TX; 2010.
45. De Vries FP. Automatic, adaptive, brightness independent contrast enhancement. *Signal Process*. 1990;21:169–182.
46. Lewis J. Fast normalized cross-correlation/fast template matching. *Vis Interface*. 1995;120–123.
47. Nelder JA, Mead R. A simplex method for function minimization. *Comput J*. 1965;7:308–313.
48. Zhong F, Wang B, Wei J, et al. A high-accuracy and high-efficiency digital volume correlation method to characterize in-vivo optic nerve head biomechanics from optical coherence tomography. *Acta Biomaterial*. 2022;143:72–86.
49. Fazio MA, Clark ME, Bruno L, Girkin CA. In vivo optic nerve head mechanical response to intraocular and cerebrospinal fluid pressure: imaging protocol and quantification method. *Sci Rep*. 2018;8:12639.
50. Feola AJ, Nelson ES, Myers J, Ethier CR, Samuels BC. The impact of choroidal swelling on optic nerve head deformation. *Invest Ophthalmol Vis Sci*. 2018;59:4172–4181.
51. Girard M, Suh JK, Hart RT, Burgoyne CF, Downs JC. Effects of storage time on the mechanical properties of rabbit peripapillary sclera after enucleation. *Curr Eye Res*. 2007;32:465–470.
52. Jan N-J, Sigal IA. Collagen fiber recruitment: a microstructural basis for the nonlinear response of the posterior pole of the eye to increases in intraocular pressure. *Acta Biomaterial*. 2018;72:295–305.
53. Jan N-J, Gomez C, Moed S, et al. Microstructural crimp of the lamina cribrosa and peripapillary sclera collagen fibers. *Invest Ophthalmol Vis Sci*. 2017;58:3378–3388.
54. Grytz R, Fazio MA, Girard MJ, et al. Material properties of the posterior human sclera. *J Mech Behav Biomed Mater*. 2014;29:602–617.
55. Grytz R, Fazio MA, Libertiaux V, et al. Age- and race-related differences in human scleral material properties. *Invest Ophthalmol Vis Sci*. 2014;55:8163–8172.
56. Holzapfel GA. Biomechanics of soft tissue. In: *The handbook of materials behavior models*. Vol. 3. 2001:1049–1063.
57. Hansen KA, Weiss JA, Barton JK. Recruitment of tendon crimp with applied tensile strain. *J Biomech Eng*. 2002;124:72–77.
58. Thornton G, Shrive N, Frank C. Ligament creep recruits fibres at low stresses and can lead to modulus-reducing fibre damage at higher creep stresses: a study in rabbit medial collateral ligament model. *J Orthop Res*. 2002;20:967–974.
59. Fratzl P. Collagen: structure and mechanics, an introduction. In: *Collagen*. Boston, MA: Springer; 2008:1–13.
60. Birch HL, Thorpe CT, Rumian AP. Specialisation of extracellular matrix for function in tendons and ligaments. *Muscles Ligaments Tendons J*. 2013;3:12.
61. Ethier CR, Johnson M, Ruberti J. Ocular biomechanics and biotransport. *Annu Rev Biomed Eng*. 2004;6:249–273.
62. Brazile B, Yang B, Voorhees A, Sigal IA. Simultaneous in-situ visualization and quantification of lamina cribrosa collagen beams and capillaries at normal and elevated IOPs. *Invest Ophthalmol Vis Sci*. 2018;59:1220–1220.
63. Midgett DE, Jefferys JL, Quigley HA, Nguyen TD. The contribution of sulfated glycosaminoglycans to the inflation response of the human optic nerve head. *Invest Ophthalmol Vis Sci*. 2018;59:3144–3154.
64. Wang B, Hua Y, Brazile BL, Yang B, Sigal IA. Collagen fiber interweaving is central to sclera stiffness. *Acta Biomaterial*. 2020;113:429–437.
65. Liu J, He X. Corneal stiffness affects IOP elevation during rapid volume change in the eye. *Invest Ophthalmol Vis Sci*. 2009;50:2224–2229.

66. McMonnies C. An examination of the hypothesis that intraocular pressure elevation episodes can have prognostic significance in glaucoma suspects. *J Optom*. 2015;8:223–231.
67. Khaw P, Shah P, Elkington A. ABC of eyes: glaucoma—1: diagnosis. *BMJ*. 2004;328:97.
68. Sigal IA, Flanagan JG, Tertinegg I, Ethier CR. Finite element modeling of optic nerve head biomechanics. *Invest Ophthalmol Vis Sci*. 2004;45:4378–4387.
69. Sigal IA, Ethier CR. Biomechanics of the optic nerve head. *Exp Eye Res*. 2009;88:799–807.